Supporting Information

Cocatalyst Designing: A Regenerable Molybdenum-Containing Ternary Cocatalyst System for Efficient Photocatalytic Water Splitting

G. Wilma Busser,[a] Bastian Mei,[b] Philipp Weide,[a] Peter C. K. Vesborg,[b] Kai Stührenberg,[c] Matthias Bauer,[c] Xing Huang,[d] Marc-Georg Willinger,[d] Ib Chorkendorff,[b] Robert Schlögl,[d] and Martin Muhler,[a,*]

[a] Laboratory of Industrial Chemistry, Ruhr-Universität Bochum, Universitätsstr. 150, 44780 Bochum, Germany, Fax: (+49)234-32-14115, E-Mail: muhler@techem.rub.de.
[b] Department of Physics, CINF. Technical University of Denmark, Fysikvej, 2800, Kongens Lyngby, Denmark.

[c] Fakultät für Naturwissenschaften, Department Chemie, Universität Paderborn, Warburger Straße 100, 33098 Paderborn, Germany.

[d] Anorganische Chemie, Fritz-Haber-Institut, Faradayweg 4-6, 14195 Berlin, Germany.

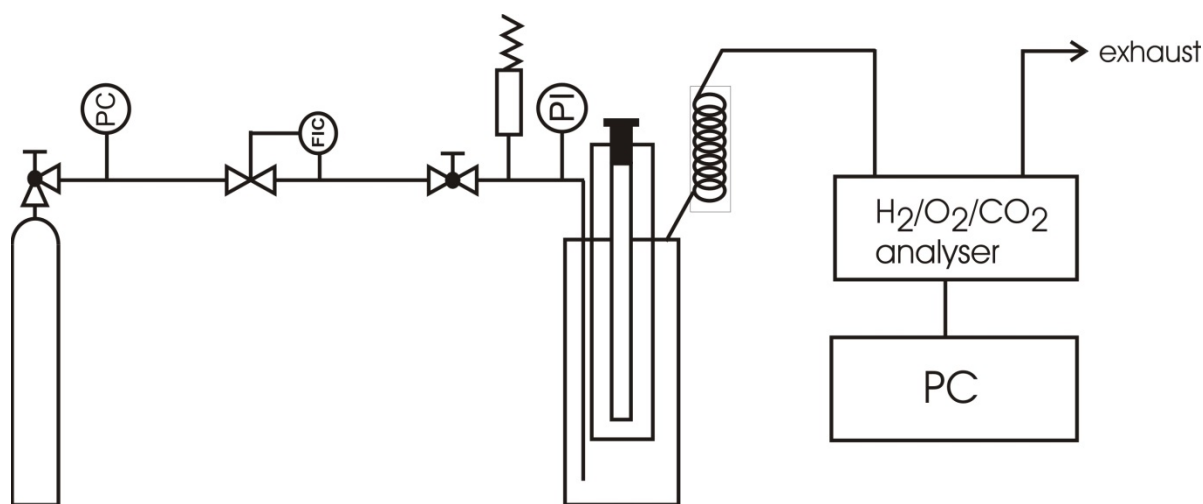[*] E-Mail: muhler@techem.rub.de

Figure S1. Continuously flushed set-up used for sequential photodeposition and water splitting.

In a typical photodeposition of the different metal oxide co-catalysts 1g of commercially available Ga_2O_3 (Chempur) is suspended in a methanolic solution 50 ml MeOH/550 ml

deionized H_2O in a home-made stirred quartz reactor with an inner irradiation-type light source (Figure S1). The apparatus was connected to a gas-dosing system equipped with a mass flow controller (Bronkhorst). The inert carrier gas (nitrogen; flows adjustable from 0 – 75 Nml/min; typical flow: 50 Nml/min) was passed through the reactor using a frit. Irradiation of the suspension is performed using a mercury lamp (Peschl, Hg immersion lamp TQ, power adjustable from 0 – 700 W, irradiance see Figure S2) and evolving gases are analyzed on-line using a 3-channel analyzer (Emerson) equipped with detectors for the determination of the concentration of hydrogen (thermal conductivity detector, detection limit 100 ppm), oxygen (paramagnetic detector, detection limit 100 ppm) and carbon dioxide (IR detector, detection limit 10 ppm). The measured concentrations were recorded using a PC equipped with LabView software.

First, flushing with nitrogen for at least 1 h degasses the Ga_2O_3 containing-suspension. Afterwards, the suspension is irradiated for 1 h and H_2 and CO_2 evolution due to methanol reforming is detected to ensure reproducibility of the performed experiments. Subsequently, the light is switched off and the desired amount of co-catalyst precursor is added to the suspension (e.g. as shown in Figure S4 Na_2MoO_4). The photodeposition of the co-catalyst is performed after thoroughly purging the reactor with N_2 to remove traces of air. During photodepositon evolving gases are recorded as described above.

Determination of the photon flux

The total light intensity of the light source (inner irradiation type, Hg lamp with polychromatic light (line spectrum 250-700 nm, Figure S2)) was determined using a physical actinometer (Nova II equipped with PD300UV supplied by Ophir) at the point where the light enters the liquid. This intensity amounted 59 (+/-4) mW/cm^2. The irradiation area was estimated by assuming a capsule-shaped emission profile (diameter: 5.35 cm; length: 15 cm) resulting in an area of 342 cm^2. From the spectrum of the lamp (relative intensity as a function of the wavelength) the actual intensity as a function of wavelength was calculated using the measured total intensity. Subsequently, the photonflux as a function of wavelength was calculated using the wavelength dependent energy pro photon (h x c x N_a/λ where h= Planck constant, c= speed of light, N_a= Avogadro constant, λ = wavelength). The sum of the photon fluxes of the relevant part of the spectrum (250-300 nm, i.e. wavelengths of photons that theoretically can be absorbed by Ga_2O_3) was determined to be 9.4 (+/- 0.6) x 10^{-6} mol/s (equals 34 (+/- 4) mmol/h).
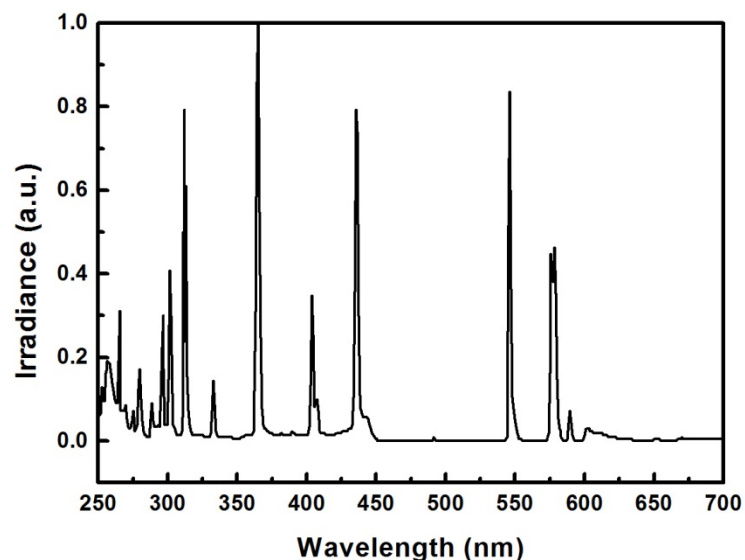
Figure S2. Normalized irradiance spectra of the Hg-discharge lamp used in the liquid phase water splitting set-up.
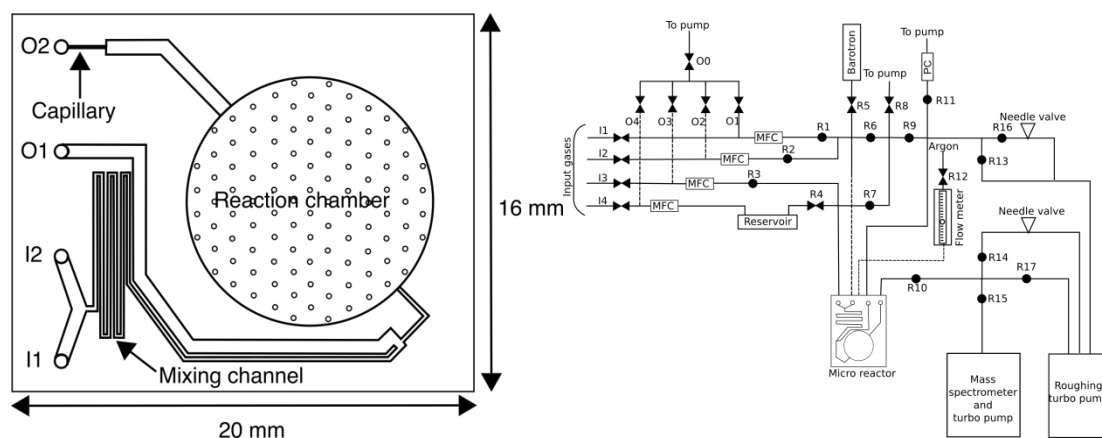

Figure S3. Schematic picture of the μ-reactor used for the backward reaction experiments.

CuO_z/MoO_x modified Ga_2O_3

$CuO_z/MoO_x/Ga_2O_3$ was prepared in analogy to the synthesis of CuO_z/CrO_y-modified Ga_2O_3.[1] The Mo loading was fixed to a loading of 0.16 wt% Mo. Subsequently, various amounts of CuO_z were photodeposited. It should be noted that the Mo loading was fixed to prepare photocatalysts that are directly comparable to previously reported binary CuO_z/CrO_y-modified Ga_2O_3 photocataltysts.[1] Thus, the Mo loading (0.16 wt%) used here was chosen to correspond to the molar loading of Cr (0.09 wt%) that had been used previously.[1] After photodeposition in methanolic solution the suspension was filtered and the particles were freeze-dried overnight without additional calcination. $CrO_y/MoO_x/Ga_2O_3$ and $CuO_z/CrO_y/MoO_x/Ga_2O_3$ were prepared by photodeposition of CrO_y and CuO_z on MoO_x/Ga_2O_3 in water as indicated in the text.

The H_2 evolution due to aqueous methanol reforming during photodeposition of CuO_z on MoO_x/Ga_2O_3 in 10% CH_3OH/H_2O solution shows a strong dependence on the Cu loading (Figure S4), and an increase in the H_2 evolution rate with increasing Cu loading can be observed. In fact, the influence of the Cu loading observed for $CuO_z/MoO_x/Ga_2O_3$ photocatalysts closely resembles the behavior observed for $CuO_z/CrO_y/Ga_2O_3$. As mentioned above, MoO_x-modified Ga_2O_3 was able to split water into H_2 and O_2 without any sacrificial agent. However, increasing Cu loadings were found to be detrimental to the overall water splitting activity of the $CuO_z/MoO_x/Ga_2O_3$ photocatalysts, whereas an optimum activity for overall water splitting was observed for $CuO_z/CrO_y/Ga_2O_3$ with a Cu loading of 0.66 wt% (Figure S5).
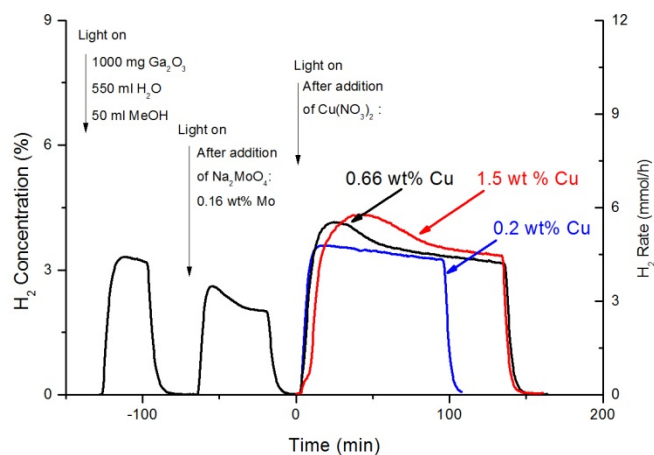

Figure S4. H_2 evolution during the photodeposition of CuO_z on MoO_x/Ga_2O_3 (0.16 wt% Mo) in 550 ml H_2O and 50 ml methanol.
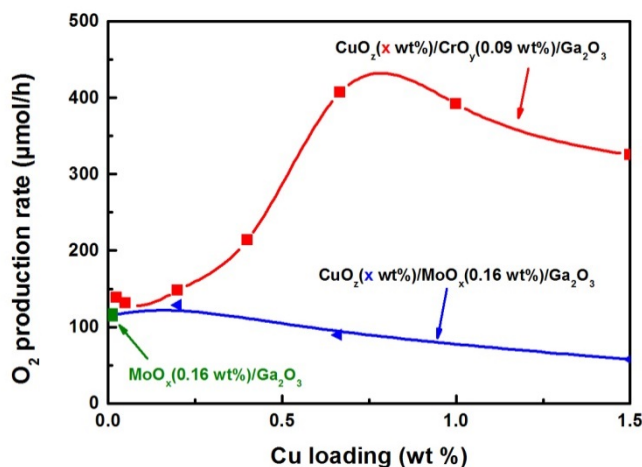

Figure S5. Dependence of the O_2 evolution rate in direct water splitting on the Cu loading for $CuO_z/CrO_y/Ga_2O_3$ (squares, adapted from ref. [9]) and for $CuO_z/MoO_x/Ga_2O_3$ (diamonds) during overall water splitting. While the Cr loading was fixed to 0.09 wt%, the Mo loading was fixed to 0.16 wt% to achieve equal molar amounts. For all experiments the liquid phase water splitting

set-up was used and 300 mg of photocatalyst were suspended in 550 ml pure water. Irradiation with the high-pressure Hg lamp was performed at a power of 250 W.
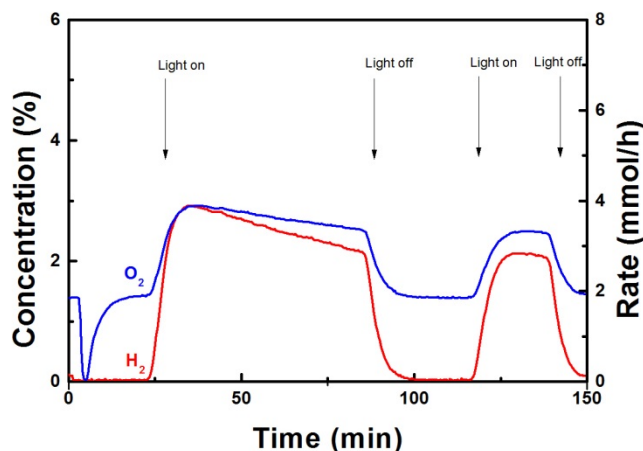

Figure S6. Liquid phase overall water splitting performed with a $CuO_z/CrO_y/MoO_x/Ga_2O_3$ photocatalyst in a carrier gas of 1% O_2/N_2. The lamp power of the high-pressure Hg lamp was adjusted to 500 W.
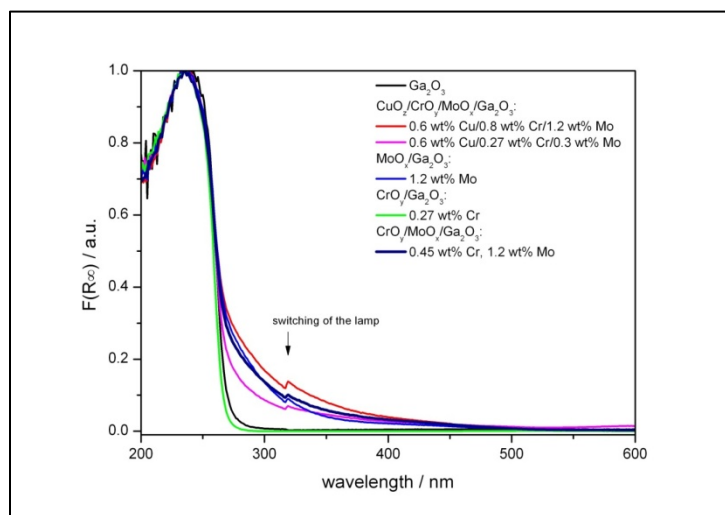

Figure S7. UV-Vis spectra of different $CuO_z/CrO_y/MoO_x$ –modified Ga_2O_3 photocatalysts.

The DR-UVVIS spectrum of pure Ga_2O_3 clearly shows that absorption occurs at wavelengths below 300 nm. The corresponding band gap was estimated to be 4.6 eV. This value is in accordance with the value reported for pure Ga_2O_3.[2] Upon loading with molybdenum species, additional to the typical absorption feature of the spectrum of Ga_2O_3, an increase in absorption was observed in the range of 300 to 500 nm, where the absorption declined monotonously with increasing wavelength. A similar phenomenon was observed by Strunk et al.[3] when loading TiO_2 with SnO_x species. According to literature, the absorption up to 450 nm can be attributed to the presence of MoO_3 species (band gap 2.7 eV; 460 nm)[4,5] and is in accordance with our XPS measurements. Small contributions to the absorption at higher wavelengths might be caused by MoO_2 species. The metallic character of these species leads to absorption in the full visible range. The presence of chromia does not give rise to additional absorption features.
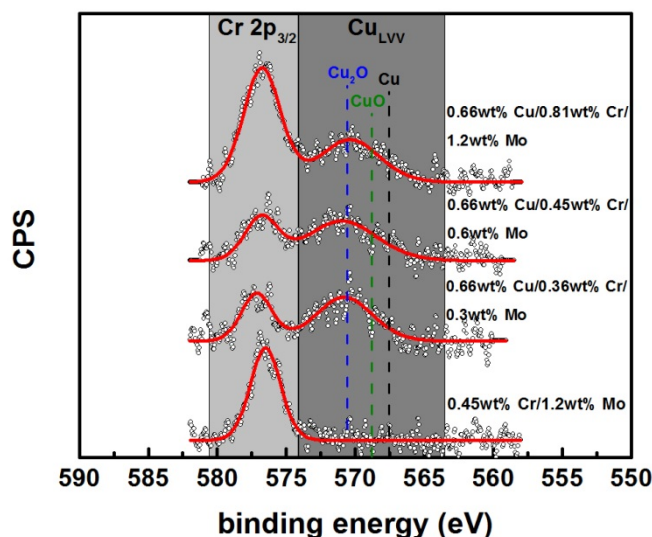
Figure S8. X-ray photoelectron spectroscopy of the Cr 2p and Cu LVV region of Ga_2O_3 photocatalysts after modification with different Mo-containing co-catalysts.
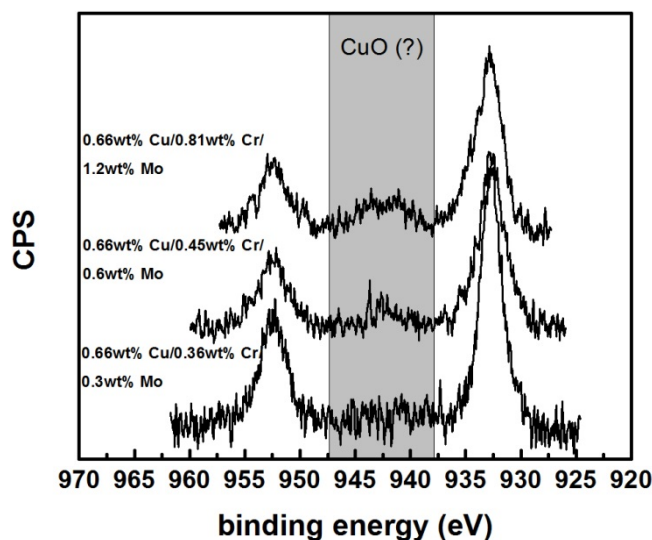

Figure S9. X-ray photoelectron spectroscopy of the Cu 2p region of Ga_2O_3 photocatalysts after modification with different Mo-containing co-catalysts.

The results of the copper K-edge XANES analysis are reflected in the EXAFS parameters, which were obtained by fitting the experimental data with theoretical models. The samples show slightly different nearest neighbor Cu-O distances: 1.97 Å for CuO_z/Ga_2O_3 (fresh), 1.94 Å for $CuO_z/CrO_y/Ga_2O_3$ (fresh), 1.91 Å for $CuO_z/CrO_y/Ga_2O_3$ (after 10 h TOS) and 1.93 Å for $CuO_z/CrO_y/MoO_z/Ga_2O_3$ (after 15 h TOS). The Cu-O distances in $CuGa_2O_4$, CuO and Cu_2O are 1.99 Å, 1.95 Å and 1.86 Å respectively. Therefore, the experimentally determined Cu-O distance is in agreement with the mixture of species as determined from the LC-XANES fit, since it has to be taken into account that size effects will affect the distances and no exact comparison to bulk crystal structures is possible. The found Cu-O coordination number of 4.9 in $CuO_z/CrO_y/Ga_2O_3$

(fresh) reflects the significant contribution of $Cu(II)Ga_2O_4$ and CuO, since in both compounds Cu is mainly coordinated in an octahedral environment.

The increased fraction of Cu_2O in $CuO_z/CrO_y/Ga_2O_3$ (after 10 h TOS) reduces the coordination number. This effect is enhanced by the fact that a larger fraction of $Cu(0)$ is present. Despite the numeric value of the Cu-Cu shell, the contribution of Cu can easily be deduced from the increased signal at around 2.5 Å in the Fourier transformed EXAFS function in Figure S11. Considering the fact that only 30% of the Cu centers are located in a Cu species, a Cu particle size of around 12 Å can be roughly estimated.

In contrast, the sample $CuO_z/CrO_y/MoO_x/Ga_2O_3$ (after 15 h TOS) exhibits a significant similarity to $CuO_z/CrO_y/Ga_2O_3$ (fresh), although the spectrum in Figure S8 appears to be slightly more damped. This can be attributed to a larger degree of disorder, especially in the more distanced shells. In view of this fact, the obtained coordination numbers agree rather well and correspond to the deduced fractions of the LC- XANES fit.

In agreement with the LC-XANES fit, the EXAFS spectrum of CuO_x/Ga_2O_3 is dominated by a Cu^0 character (Figure S11, Table S1). Only one Cu-O shell with an average coordination number of 0.9 can be fitted beside a typical model for bulk copper. In principle, this reflects the results from the LC-XANES fit, however, a larger Cu-O contribution would be expected in Table S1 according to the results in Table 3. Here, the EXAFS results are considered more reliable, since particle size effects are not accounted for in the LC-XANES fit, but the EXAFS results indicate rather small particles. It can thus be concluded that for sample CuO_z/Ga_2O_3 the amount of oxidic species is overestimated. Regarding the particle sizes from the EXAFS spectra it has to be stated that the first Cu-Cu coordination shell indicates a particle size of around 10 Å, while the second and third Cu-Cu contributions are more characteristic of particles of around 20 Å diameter, assuming spherical particles are present. This apparent contradiction can be explained by an at least bimodal size distribution, or in a more general sense, a large spread of particle sizes.
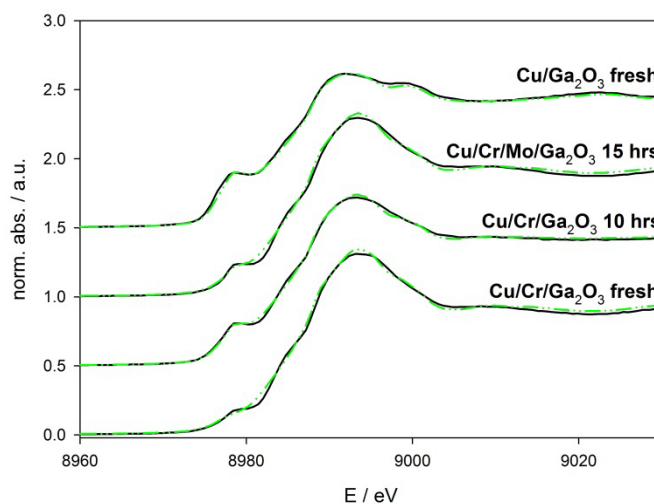

Figure S10. Experimental XANES spectra (black solid line) of the samples measured samples together with the resulting spectra of the LC-XANES fit (dotted dashed green line).
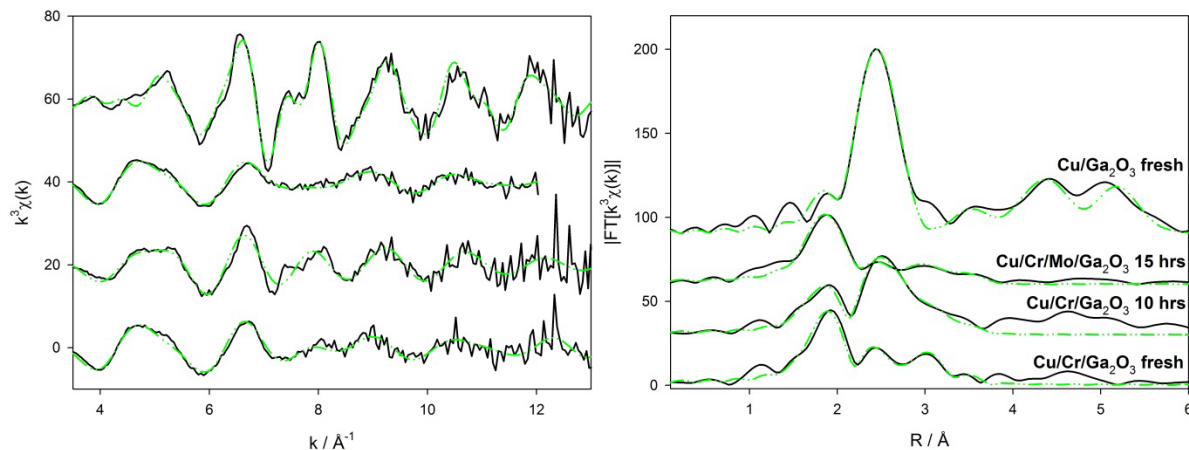
Figure S11. Experimental (solid black line) and fitted (dotted dashed green line) EXAFS spectra (left) and the according Fourier transformed functions (right) of the samples CuO_z/Ga_2O_3 fresh, B. $CuO_z/CrO_y/Ga_2O_3$ (fresh), C. $CuO_z/CrO_y/Ga_2O_3$ (after 10 h TOS) and D. $CuO_z/CrO_y/MoO_x/Ga_2O_3$ (after 15 h TOS).

Table S1. Structural parameters obtained by fitting the experimental EXAFS spectra with theoretical models.

Sample	Abs-Bs[a]	N(Bs)[b]	R(Abs-Bs)[c]/ Å	σ[d]/ Å	FI[e]
CuO_z/Ga_2O_3	Cu-O	0.9±0.1	1.97±0.02	0.039±0.004	0.961
(fresh)	Cu-Cu	6.3±0.6	2.53±0.03	0.087±0.009	
	Cu-Cu	3.6±0.4	3.55±0.04	0.112±0.011	
	Cu-Cu	15.0±3.0	4.42±0.04	0.112±0.022	
	Cu-Cu	15.0±3.0	5.25±0.05	0.110±0.022	
$CuOz/CrOy/Ga_2O_3$	Cu-O	4.9±0.5	1.94±0.02	0.092±0.009	1.921
(fresh)	Cu-Cu	0.5±0.1	2.51±0.03	0.045±0.005	
	Cu-Ga	0.4±0.1	2.93±0.03	0.032±0.006	
	Cu-O	3.6±0.7	3.41±0.03	0.102±0.020	
$CuO_z/CrO_y/Ga_2O_3$	Cu-O	3.6±0.4	1.91±0.02	0.097±0.010	0.290
(after 10 h TOS)	Cu-Cu	2.2±0.2	2.51±0.03	0.081±0.008	
	Cu-Ga	1.2±0.1	2.93±0.03	0.097±0.019	
	Cu-O	4.0±0.8	3.41±0.03	0.107±0.021	
$CuO_z/CrO_y/MoO_x/Ga_2O_3$	Cu-O	4.5±0.5	1.93±0.02	0.092±0.009	0.916
(after 15 h TOS)	Cu-Cu	0.3±0.1	2.52±0.03	0.045±0.005	
	Cu-Ga	0.3±0.1	2.92±0.03	0.039±0.008	
	Cu-O	4.7±0.4	3.44±0.03	0.112±0.022	

a) Abs=X-ray absorbing atom, BS=backscattering atom, b) number of backscattering atoms, c) distance between absorbing and backscattering atom, d) Debye-Waller-like factor, e) Quality of fit.

In order to support the deduced chromium oxidation states, high energy resolution hard X-ray spectroscopy at the chromium K-edge was performed. Core to core X-ray emission (ctc XES) and high energy resolution fluorescence detected XANES (HERFD-XANES) spectra were recorded at beamline ID26 of the ESRF (Grenoble) using a Johann type spectrometer.[6] Figure S12 shows the spectra for the samples 0.6 wt% Cu/0.45 wt% Cr/ 0.6 wt% Mo and 0.6 wt% Cu/0.8 wt% Cr/ 1.2 wt% Mo. The HERFD-XANES spectra show the typical form of Cr(III).[7] The ctc XES spectra reflect the total spin at the chromium center. Although exact analysis

requires elaborated calculations, comparison with literature confirms the oxidation state of Cr(III), since a satellite of considerable intensity is found at 5934 eV that is separated by 13 eV from the main peak.[8,9]
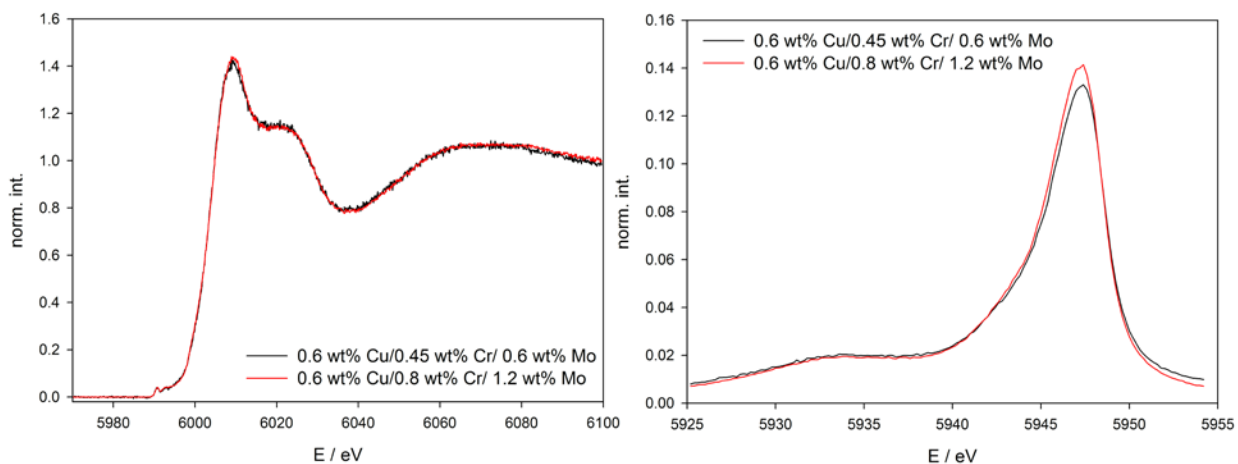

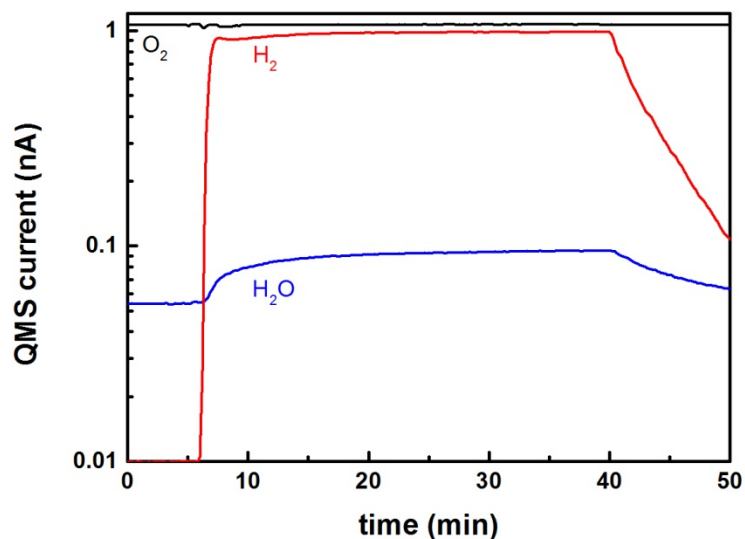**Figure S12.** HERFD-XANES (left) and ctc XES (right) spectra of the samples mentioned.

Figure S13. Back reaction of H_2 and O_2 performed in a gas phase μ-reactor at 298 K without catalyst.

REFERENCES

(1)   Busser, G. W.; Mei, B.; Pougin, A.; Strunk, J.; Gutkowski, R.; Schuhmann, W.; Willinger, M.-G.; Schlögl, R.; Muhler, M. *ChemSusChem* **2014**, *7*, 1030–1034.

(2)   Mohamed, M.; Unger, I.; Janowitz, C.; Manzke, R.; Galazka, Z.; Uecker, R.; Fornari, R. *J. Phys. Conf. Ser.* **2011**, *286*, 012027-012027-9.

(3)   Oropeza, F. E.; Mei, B.; Sinev, I.; Becerikli, A. E.; Muhler, M.; Strunk, J. *Appl. Catal. B Environ.* **2013**, *140-141*, 51–59.

(4)   Dieterle, M.; Weinberg, G.; Mestl, G. *Phys. Chem. Chem. Phys.* **2002**, *4*, 812–821.

(5)   Griffin, J.; Watters, D. C.; Yi, H.; Iraqi, A.; Lidzey, D.; Buckley, A. R. *Adv. Energy Mater.* **2013**, *3*, 903–908.

(6)   Glatzel, P.; Bergmann, U. *Coord. Chem. Rev.* **2005**, *249*, 65–95.

(7)   Berry, A. J.; O'Neill, H. S. C. , *A XANES determination of the oxidation state of chromium in silicate glasses*; *American Mineralogist* **2004**, *89*, 790-798.

(8)   Lenglet, M.; Sakout, M.; Dürr, J.; Wrobel, G. *Spectrochim. Acta Part A Mol. Spectrosc.* **1990**, *46*, 1101–1106.

(9)   Tsutsumi, K.; Nakamori, H. *J. Phys. Soc. Japan* **1968**, *25*, 1418–1423.